Cell Systems

Article

Entrainment and multi-stability of the p53 oscillator in human cells

Graphical abstract

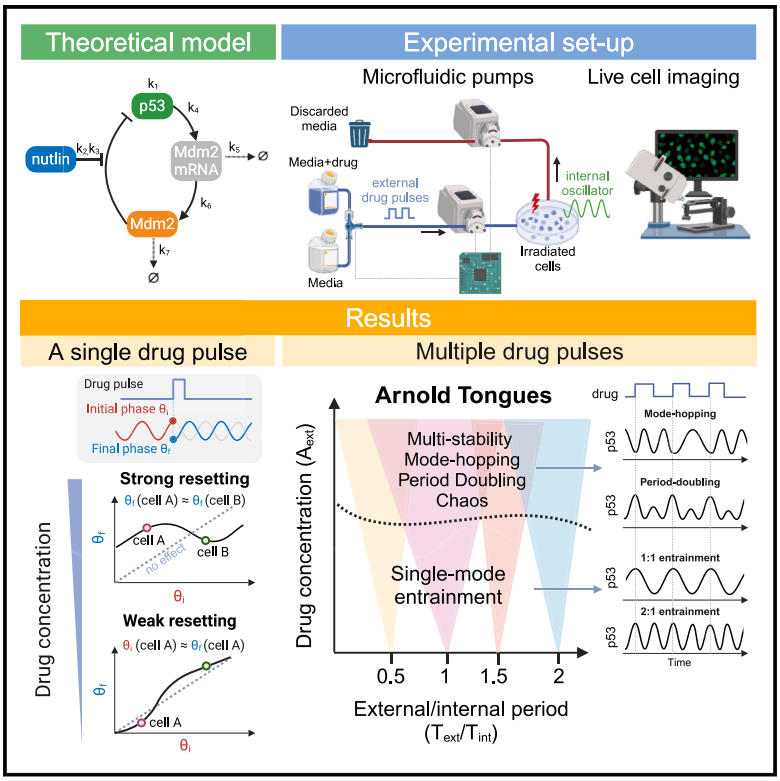

Authors

Alba Jiménez, Alessandra Lucchetti, Mathias S. Heltberg, ..., Ashwini Jambhekar, Mogens H. Jensen, Galit Lahav

Correspondence

mhjensen@nbi.ku.dk (M.H.J.), galit@hms.harvad.edu (G.L.)

In brief

The theory of synchronization and entrainment was applied to quantify and model the response of the p53 oscillator to external drug pulses of various strengths and periods. Single-cell data allowed deriving multiple Arnold tongues, featuring numerous entrainment modes and complex non-linear dynamics of p53, including mode hopping, period doubling, and chaos.

Highlights

- Entrainment in the p53 system was studied using theory and live-cell imaging
- The p53 oscillator can be reset and locked to a wide range of entrainment modes
- Phase response curves and Arnold tongues were derived from p53 single-cell traces
- Non-linear p53 dynamics, such as mode hopping, period doubling, and chaos, were detected

Jiménez et al., 2024, Cell Systems *15*, 956–968
October 16, 2024
https://doi.org/10.1016/j.cels.2024.09.001

CellPress

CellPress

Cell Systems

Article

Entrainment and multi-stability of the p53 oscillator in human cells

Alba Jiménez,[1,3] Alessandra Lucchetti,[1,2,3] Mathias S. Heltberg,[1,2,3] Liv Moretto,[2] Carlos Sanchez,[1] Ashwini Jambhekar,[1] Mogens H. Jensen,[2,*] and Galit Lahav[1,4,*]

[1]Department of Systems Biology, Blavatnik Institute at Harvard Medical School, Boston, MA 02115, USA
[2]Niels Bohr Institute, University of Copenhagen, Copenhagen 2100, Denmark
[3]These authors contributed equally
[4]Lead contact
*Correspondence: mhjensen@nbi.ku.dk (M.H.J.), galit@hms.harvad.edu (G.L.)
https://doi.org/10.1016/j.cels.2024.09.001

SUMMARY

The tumor suppressor p53 responds to cellular stress and activates transcription programs critical for regulating cell fate. DNA damage triggers oscillations in p53 levels with a robust period. Guided by the theory of synchronization and entrainment, we developed a mathematical model and experimental system to test the ability of the p53 oscillator to entrain to external drug pulses of various periods and strengths. We found that the p53 oscillator can be locked and entrained to a wide range of entrainment modes. External periods far from p53's natural oscillations increased the heterogeneity between individual cells whereas stronger inputs reduced it. Single-cell measurements allowed deriving the phase response curves (PRCs) and multiple Arnold tongues of p53. In addition, multi-stability and non-linear behaviors were mathematically predicted and experimentally detected, including mode hopping, period doubling, and chaos. Our work revealed critical dynamical properties of the p53 oscillator and provided insights into understanding and controlling it. A record of this paper's transparent peer review process is included in the supplemental information.

INTRODUCTION

Oscillations can be found across a wide range of biological systems and play important roles in regulating gene expression and various cellular behaviors.[1–7] The phenomenon in which one oscillator adopts the period of another oscillator is called entrainment and is essential for many biological functions,[8] including synchronizing internal cellular processes (e.g., entrainment of the cell-cycle oscillator with the circadian oscillator),[9–11] coordination between cells (e.g., cardiac cells synchronize their oscillations to provide heart contraction),[12] and synchronizing organisms' physiology with their surrounding rhythms (e.g., the sleep-wake cycles of the circadian clock entrain to light-dark cycles).[13–16] In addition, oscillating transcription factors can be entrained by external oscillators, leading to changes in their function. For example, externally applied periodic tumor necrosis factor alpha (TNF-α) stimulation entrains the nuclear-cytoplasmic shuttling cycle of the pro-inflammatory transcription factor nuclear factor κB (NF-κB), leading to a more robust transcriptional response.[17]

To study entrainment, a system is typically set up with an autonomous internal oscillator that is perturbed by an external oscillator, with a specific periodicity and strength. Initially, the external input can hit the autonomous oscillator at a period mismatch. When entrainment occurs, the mismatch between both signals progressively decreases and a stable phase relationship can be established. At that point, the entrained oscillator goes through p cycles for every q cycles of the external signal, leading to p:q period locking (or mode locking).[18,19] Although simple entrainment refers to synchronization of the autonomous oscillator to the external input in a 1:1 ratio, other higher-order entrainment modes can be observed. For instance, the internal oscillator could adopt double or half the frequency of the external one (2:1 and 1:2 entrained mode, respectively). When the strength of the external signal is above a critical value, the internal oscillator may become phase locked to different frequencies, depending on its initial condition, leading to multiple stable entraining modes (multi-stability). In the presence of noise, the oscillator can thus jump between different stable states, a phenomenon known as "mode hopping."[20–22] In addition, the system may also undergo a type of bifurcation known as period doubling (or halving).[23] This phenomenon occurs when a new trajectory emerges from an existing periodic trajectory—with the emerging one having double (or half) the period of the original. A period-doubling cascade (i.e., an infinite sequence of period-doubling bifurcations) is a common route by which dynamical systems develop chaotic behaviors.[24,25]

The ability of a system to entrain depends on the initial period mismatch (detuning) and the strength of the external perturbation. Conversely, if the detuning is large, a strong signal is required for entrainment. Maps describing the regions of parameter space that give rise to entrained states as a function

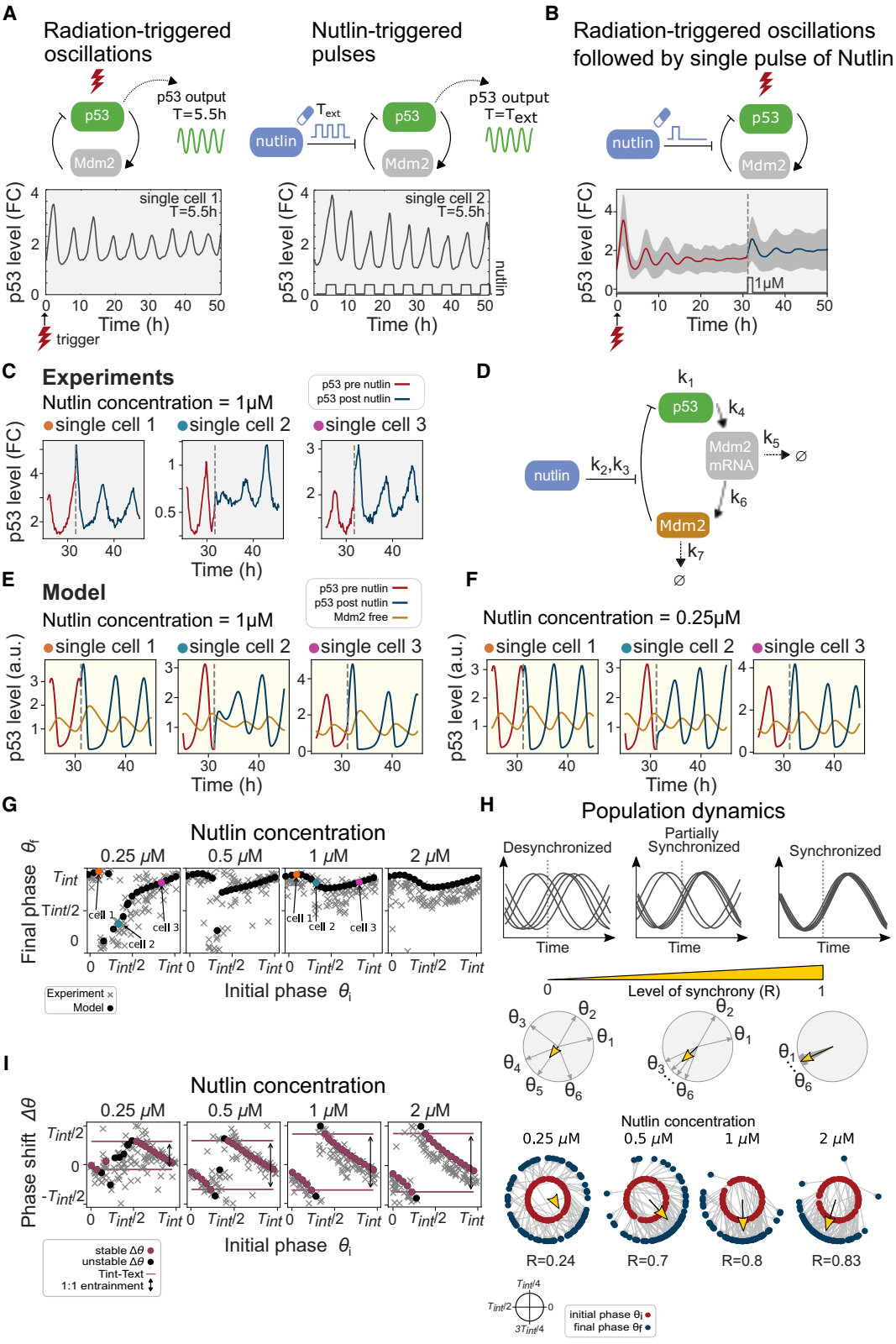

Figure 1. Phase response curves of the p53 system show phase resetting and predict entrainment

Experimental versus model traces are distinguished with gray and yellow backgrounds, respectively. (A) A single-cell trace of p53 oscillations with a 5.5-h period after 10 Gy radiation (left). A single-cell trace of an unirradiated cell subjected to oscillating nutlin concentrations with T_{ext} = 5.5 h (right).

(legend continued on next page)

of the strength of the external input against its period are commonly known as Arnold tongues.[25] Such maps illustrate the conditions under which the autonomous oscillator will entrain at a given mode. As the strength of the external input increases, the system becomes increasingly entrainable, even when the periods of the external input are far from the natural period, resulting in broadening of the tongue. Above a critical value of input strength, the tongues may overlap, resulting in regions where complex dynamics (multi-stability, mode hopping, period doubling, and chaos) can occur.[19,22,25] Arnold tongues have been described in numerous physical systems, from fluids[26] and semiconductors[27] to sliding charge-density-waves.[28] In biological settings, the identifications of Arnold tongues are still sparse. Leon Glass observed entrainment within cardiac rhythms[29] and in bacterial colonies two Arnold tongues have been identified.[30] At the single-cell level, the oscillations of the transcription factor NF-κB perturbed by an external oscillating TNFα signal, exhibited a few Arnold tongues[17,31] and the phenomenon of mode hopping between two tongues was observed.[22] In developing mice embryos, the periodic formation of somites perturbed by an external oscillating signal revealed the fundamental 1:1 tongue.[32] A series of multiple entrained states represented by multiple Arnold tongues have yet to be observed in biological systems.

In this study, we focused on the transcription factor p53 as a model system for studying entrainment of a biological oscillator. The tumor suppressor p53 is induced by various cellular stresses.[33] In response to DNA double-strand breaks (DSBs), p53 levels oscillate in cell cultures and *in vivo* with a robust periodicity of 5.5 h in human and 2.75 h in mice.[4,34–38] p53 oscillations arise from a negative feedback loop between p53 and its transcriptional target MDM2, an E3 ubiquitin ligase that initiates p53 degradation.[39–43] Small molecule inhibitors of Mdm2 stabilize the p53 protein and, in combination with the induction of DSB, switch p53's oscillatory behavior into sustained behavior. Alteration of p53 dynamics was shown to impact gene expression programs and consequently cellular outcomes.[44–46]

Here, we investigated the response of p53 oscillations to externally controlled pulses of the Mdm2 inhibitor, the drug Nutlin-3a.[47] Guided by the theory of synchronization and mathematical modeling, we developed an experimental system that can test the ability of the p53 oscillator to entrain to different external frequencies and coupling strengths, represented by the periodic delivery of various nutlin concentration. We acquired live single-cell imaging of p53 dynamics and used a simple ODE model to compute, predict, and validate the phase response curve (PRC) and Arnold tongues of p53. The overlap between tongues prompted us to identify several complex non-linear dynamical behaviors, including mode hopping, period doubling, and chaos. Our findings offer new ways to understand and control the complex dynamics of the p53 oscillator and suggest that entrainment in the p53 system may be a critical mechanism to ensure coordination of multiple programs affecting cellular outcomes. This work also presents one of the few experimental observations of chaos in a biological oscillator.

RESULTS

p53 oscillations can be reset by an external stimulus

To investigate the dynamical properties of p53, and whether it can be entrained, we monitored how p53's natural oscillations, triggered by DNA damage, respond to an external stimulus. A microfluidic device was set up to quickly and efficiently flow media in and out of cell culture while cells were imaged. This device allowed delivery of Nutlin-3a, a small molecule that stabilizes p53 by inhibiting its negative regulator Mdm2. p53 dynamics were monitored in human MCF7 cells by fluorescence time-lapse imaging of an integrated p53-YFP reporter. MCF7 cells express wild-type p53 and Mdm2. In addition, p53 oscillations in response to DNA damage were originally discovered in this line[4,34,37] and later observed in many other human and mice lines[36,48,49] as well as *in vivo*.[35,38] Furthermore, fluorescently tagged p53 was previously shown to mimic the dynamics of endogenous wild-type p53 in this line.[4,37,44] In our experimental system, DNA damage resulting from irradiation (IR) also led to the stereotypical p53 oscillations with a period of 5.5 h. Pulses of nutlin triggered p53 oscillations with a period that matched that of the stimulus (Figures 1A and S1).

We next tested the effect of a single pulse of nutlin on the natural p53 oscillations induced by IR. At the population level, p53 oscillations following IR appeared to dampen over time due to progressive desynchronization. At 30 h, we delivered a single 40-min pulse of nutlin at 1 μM concentration. This led to resynchronization of p53 oscillations within the population (Figure 1B). In addition, individual cells showed an immediate peak in p53 after nutlin addition, regardless of their oscillation phase at the time of addition, suggesting that their phases had been reset (Figure 1C). In principle, a single-pulse perturbation can reset the phase of the ongoing oscillations, depending on the stimulus magnitude and the phase of the internal oscillator at the time of

(B) Mean p53 trace (bold line) ± SD (shaded areas) of irradiated cells before (red) and after (blue) treatment with a single 40-min pulse of 1 μM nutlin.
(C) Experimental traces of three irradiated cells that were treated with a nutlin pulse at three different phases. Experimental p53 levels are presented in fold change (FC).
(D) Schematic illustration of the network regulating p53 dynamics.
(E) Simulation of three irradiated cells that were treated with a high dose (1 μM) of a nutlin pulse at three different phases.
(F) Simulation of three irradiated cells that were treated with a low dose (0.25 μM) of a nutlin pulse at similar phases as the cells in (E).
(G) Phase transition curves (PTCs) calculated from the experimental traces (gray crosses) and from the model (black dots) for increasing values of nutlin concentration. The number of single cells manually tracked for each experiment is in Table S2.
(H) Top: illustration demonstrating different levels of synchrony between individual oscillating cells. Vertical dotted line—time when synchrony is measured. Middle: each oscillatory trace is viewed as a vector originating at the center of the circle and pointing at the oscillator's phase when synchrony is measured (dotted line of top panel). The sum of individual vectors results in a vector (yellow arrow) whose length R represents the level of synchrony. Bottom: initial phases (red) and final phases (blue) represented in the unit circle. The order parameter R shows increasing level of synchrony for increasing nutlin concentrations.
(I) Phase response curves (PRCs) at different nutlin concentrations, with double-headed arrows indicating regions where requirements for 1:1 entrainment are fulfilled.

stimulation.[24] To determine the requirements of these parameters for phase resetting in the p53 system, we simulated p53 dynamics using the following ODE model[50] (Figure 1D):

$$\frac{dp53}{dt} = k_1 - k_2(t)\frac{Mdm2\,p53}{k_3+p53}$$

$$\frac{dMdm2_{mRNA}}{dt} = k_4\,p53^2 - k_5\,Mdm2_{mRNA}$$

$$\frac{dMdm2}{dt} = k_6\,Mdm2_{mRNA} - k_7\,Mdm2$$

p53, $Mdm2_{mRNA}$, and *Mdm2* are the concentration of p53, Mdm2-mRNA, and Mdm2 protein, respectively; p53 is produced at a fixed rate (k_1) and degraded following binding to Mdm2 through a saturated degradation process (k_2, k_3). Mdm2-mRNA production is proportional (k_4) to the square of the p53 level, to account for the multiple p53-binding sites in Mdm2 promoter. Mdm2-mRNA is then degraded through a first-order decay process (k_5). Mdm2 protein is produced proportionally to Mdm2-mRNA (k_6) and degraded through a first-order decay process (k_7). Administering a pulse of nutlin at time T_{ON} and washing it at time T_{OFF} is included in the model via the parameter k_2 undergoing exponential decay (see STAR Methods and Table S1).

We used the model to simulate cells at different phases of p53 oscillations responding to a range of nutlin concentrations. At high nutlin concentration (1 μM), cells were predicted to show an immediate peak in p53 regardless of their initial phase, suggesting that all were amenable to phase resetting (Figure 1E). When a cell receives the nutlin pulse at the trough of the p53 oscillation, (Figures 1E, middle), p53 approaches the unstable fixed point in the center of the limit cycle. As a result, the oscillations were initially suppressed to near-zero amplitude before gradually growing back to their unperturbed value. This predicted behavior matched the experimental traces (Figure 1C, middle). A very weak resetting was predicted to occur at low (0.25 μM) nutlin doses (Figure 1F). These results suggest that the magnitude of the stimulus, not the phase of the internal oscillator, is key in determining the potential of the p53 internal oscillator to reset.

To validate these model predictions, we experimentally tested the effect of the stimulus strength on p53 phase resetting. We monitored the dynamics of p53 in response to a nutlin pulse of 40 min across a range of concentrations delivered 30 h after IR. We then plotted the phase transition curves (PTCs), which represent the resulting final-phase θ_f as a function of initial-phase θ_i(Figure 1G). As predicted, at high nutlin concentrations (1 and 2 μM), phase resetting occurred regardless of the initial phase, while a weak resetting occurred at the low concentrations (0.25 μM) (Figure 1G). At an intermediate nutlin concentration (0.5 μM), we observed a mix of reset and non-reset cells, which was partially dependent on the initial phase of the internal oscillator. Overall, the ODE-model-derived predictions of phase resetting matched the experimental data (Figure 1G), suggesting that a relatively simple mathematical model can capture the complex dynamical behavior in the p53 system, including its PRCs.

The observation of increased synchrony after nutlin addition (Figure 1B) suggested that all cells may be resetting to the same phase at saturating nutlin concentration. Transition into synchrony can be examined using concentric unit circles showing the single cells' distribution of initial (inner) and final (outer) phases (Figure 1H). Our data show that increasing nutlin concentrations indeed led to increased synchrony in the population, as indicated by the higher-order parameter *R* (Figure 1H, yellow arrows), a typical behavior for limit cycle models.[24]

Phase resetting does not only predict the ability of an oscillator to internally synchronize after a single stimulus but also, most importantly, its ability to entrain to an external pulsing rhythm.[51] Two requirements need to be fulfilled for an internal oscillator (of period T_{int}) to entrain in a 1:1 ratio to an external pulsing signal (of period T_{ext}) (see STAR Methods). Such requirements are best visualized through the PRC (Figure 1I), which illustrates phase shifts ($\Delta\theta = \theta_f - \theta_i$) as a function of the initial-phase θ_i.[52] First, there must exist θ^* such that $PRC(\theta^*) = T_{int} - T_{ext}$, allowing the phase shift to compensate for the period mismatch ($\Delta T = T_{int} - T_{ext}$) (Figure 1I). And second, the slope of the PRC at θ^* must be $-2 < PR\,C'(\theta^*) < 0$, ensuring that the entrained state is stable (Figure 1I, red [stable] versus black [unstable]). We noted that these requirements are fulfilled under all nutlin concentrations (Figure 1I, double-headed arrows), suggesting that 1:1 entrainment is expected under these conditions. In addition, the mismatch (difference between the maximum and minimum of the PRC, where both requirements are fulfilled) increases for higher doses of nutlin, suggesting that the stronger the input the more it can tolerate larger phase shifts for achieving 1:1 entrainment.

p53 can entrain to a wide range of periods

We next asked whether the natural p53 oscillations induced by IR could entrain to an external periodic nutlin input. To address this, p53 oscillations were first triggered by IR (zone 1); after several hours, cells were subjected to periodic nutlin pulses at various concentrations and periods (zone 2), and then released from nutlin treatment after a minimum of 6 nutlin pulses (zone 3) (Figure 2A; Table S2).

We first used a fixed nutlin concentration of 0.5 μM and tested the effect of various nutlin periods from 2.5 to 11 h on natural p53 oscillations. Examples of entrainment to the external signal were observed at every nutlin period (Figure 2B, upper). The ODE model closely predicted 1:1 entrainment across nutlin periods (Figure 2B, lower). When examining population-level behavior, we observed greater heterogeneity in p53 oscillations in response to a 9-h nutlin period compared with a 4-h period (Figures 2C and 2D), suggesting that external inputs with periods far from the natural p53 oscillations (5.5 h) increase cell-to-cell variation. We next monitored cells at four increasing nutlin concentrations (0.25, 0.5, 1, and 2 μM) delivered with a fixed 11-h period. At 0.25 μM, we observed high cell-to-cell variation and nearly no 1:1 entrainment. Increasing nutlin concentration led to a progressive decrease in cell-to-cell variability and to a more robust and uniformed entrained traces (Figure S2). This phenomenon, known as "frequency pulling," demonstrates how an increase in coupling strength (represented here in nutlin concentration) enables robust entrainment at frequencies far from the natural one.

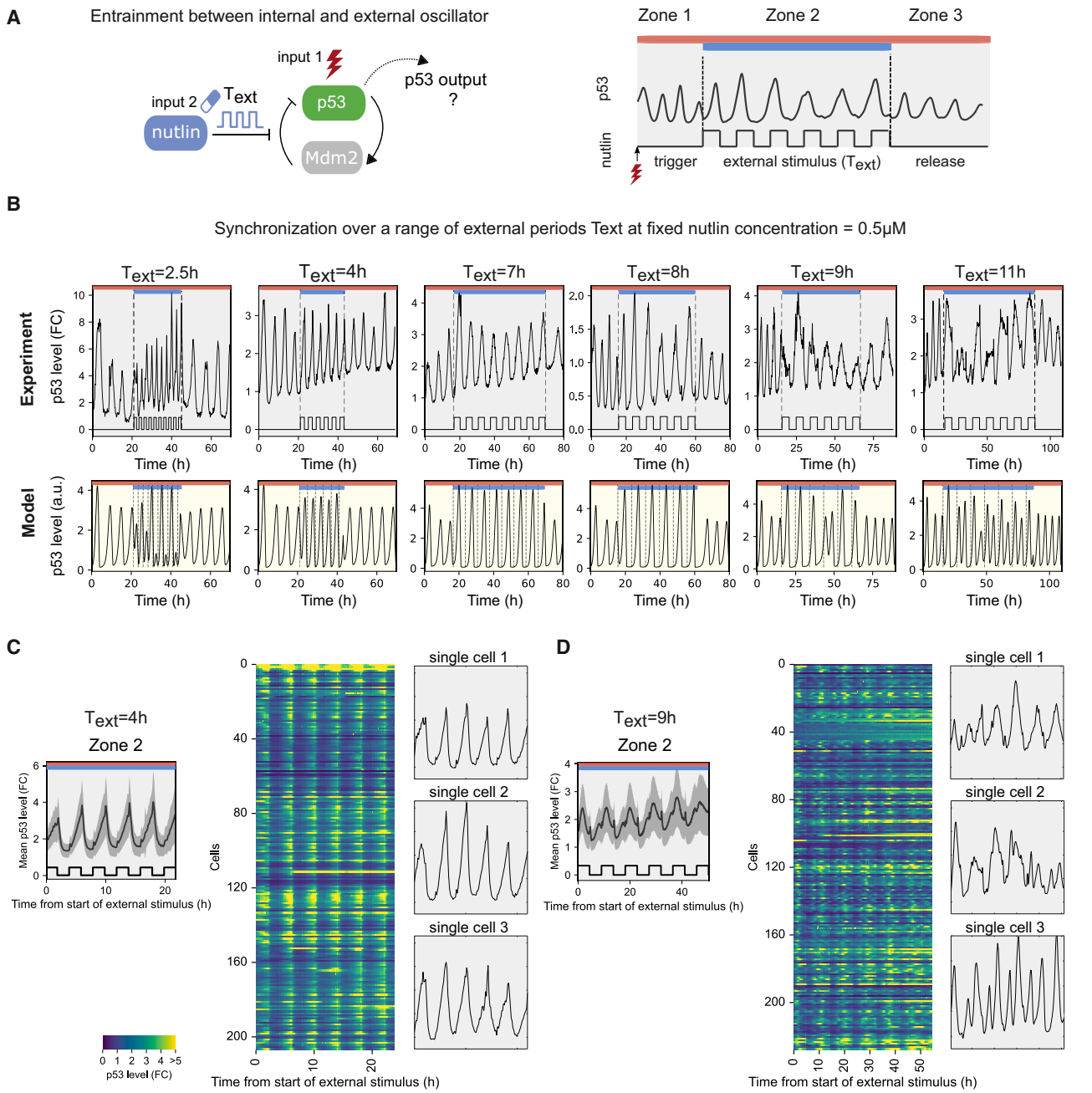

Figure 2. Entrainment of the p53 oscillator to an external periodic input

(A) Illustration of the experimental set up: cells are treated with input 1 (irradiation), leading to endogenous p53 oscillations (zone 1), then subjected to an external periodic nutlin input 2 (zone 2) and released (zone 3).

(B) Experimental (gray background) and model predicted (yellow background) traces displaying locking (1:1 entrainment) across a range of external periods T_{ext}. Each trace represents p53 dynamics in a single cell. Experimental p53 levels are presented in FC.

(C and D) p53 dynamics in zone 2 in response to 0.5 μM nutlin at T_{ext} = 4 h (C) and T_{ext} = 9 h (D). Left: mean p53 trace (bold line) ± interquartile range (shaded areas); middle: heatmaps of p53 levels over time for >200 cells manually tracked. Each row is a single cell; right: examples of p53 traces in 3 single cells.

The entrained p53 oscillator can show multiple entrainment modes

The higher variance between single-cell traces at external inputs far from the natural frequency could result from a mix of several modes of entrainment. Indeed, at a 9-h nutlin period, we found examples of cells showing periods close to either ~9 or 4.5 h, suggesting entrainment at 1:1 or 2:1 ratios (Figure 3A). We next plotted the distribution of p53 periods in cultures subjected to various nutlin periods. At nutlin periods close to the natural period of 5.5 h (4, 7, and 8 h), we observed a unimodal

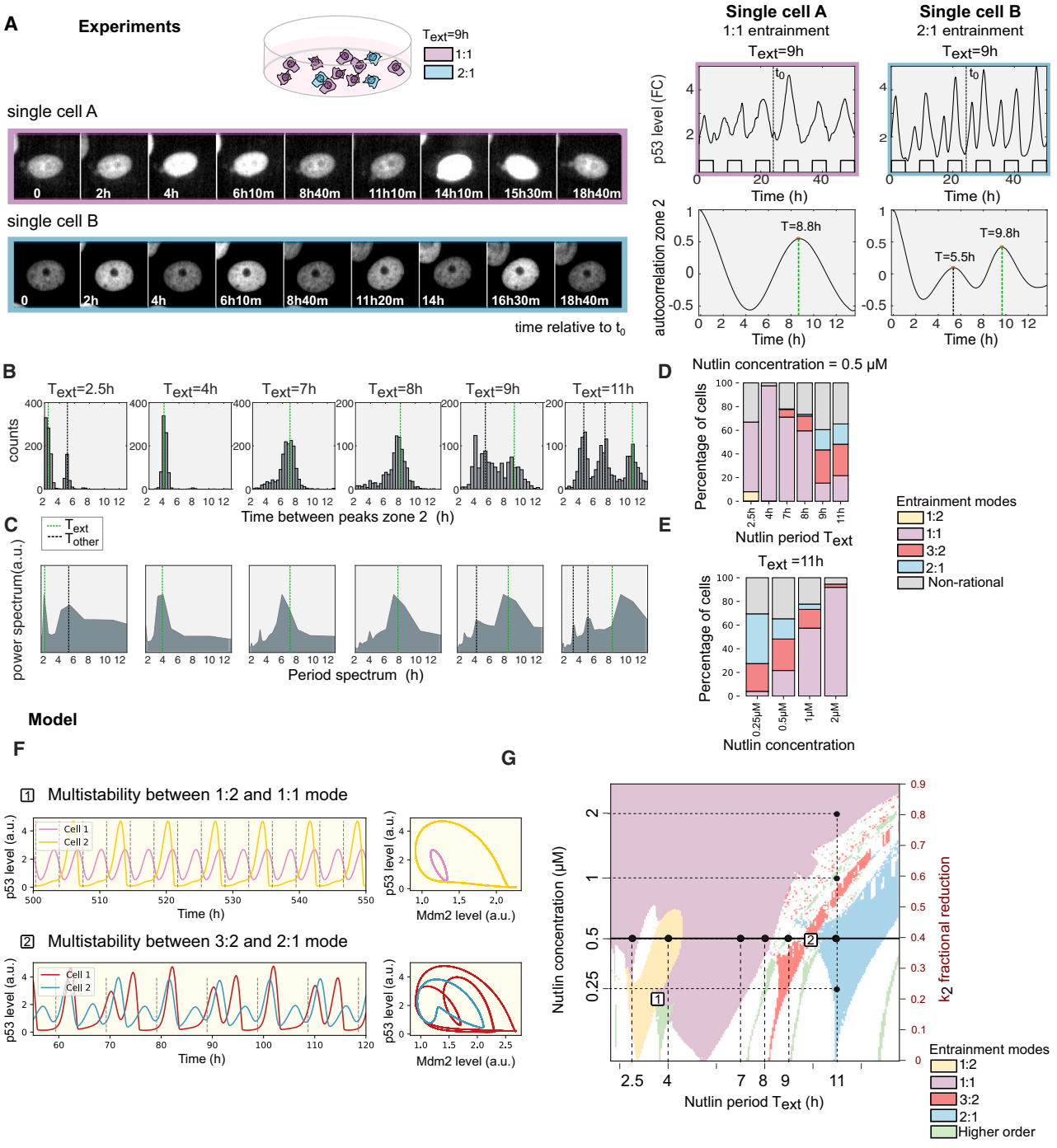

Figure 3. The p53 oscillator shows higher-order entrainment and multi-stability

(A) Images (left), quantification (top-right), and autocorrelation (bottom-right) of p53 in two cells exhibiting 1:1 or 2:1 entrainment (cell A and B, respectively) in response to 0.5 μM nutlin stimulus with T_{ext} = 9 h. The timing of imaging is relative to the t_0 indicated in top right panel. Experimental versus model traces are distinguished with gray and yellow backgrounds, respectively. Experimental p53 levels are presented in FC.

(B) Distributions of interpeak distance in zone 2 demonstrating unimodal, bimodal, and trimodal distributions for different values of T_{ext}. Each interpeak measurement corresponds to a single peak-to-peak distance in a single-cell trajectory. The number of single cells manually tracked for each experiment is in Table S2.

(C) Power spectrum distributions across different values of T_{ext} confirm unimodal, bimodal, and trimodal distributions.

(D) Percentages of cells exhibiting each entrainment mode (p:q, with p = number of internal pulses, q = number of external pulses) at a fixed nutlin concentration (0.5 μM) across T_{ext} values.

(legend continued on next page)

distribution. At nutlin periods further from the natural 5.5-h period, the distribution of p53 periods was bimodal (for 2.5 and 9 h nutlin period) or trimodal (for 11 h nutlin period) (Figure 3B). Fourier spectra revealed a single dominant frequency at nutlin periods of 4, 7, and 8 h and multiple frequencies at shorter (2.5 h) or longer nutlin periods (9 and11 h), suggesting non-trivial oscillatory dynamics (Figure 3C).

To systematically extract a cell's entrainment mode, we developed an algorithm that identifies peaks, computes the distances between successive peaks, and calculates the ratio of the number of p53 oscillations (p) to nutlin pulses (q) (see STAR Methods). We then ran the algorithm on data collected from cells in which nutlin was added at a fixed concentration (0.5 μM) under various periods and in which nutlin period was fixed (11 h) but its concentration varied. Plotting the fraction of cells exhibiting specific p:q ratios (1:1, 1:2, 3:2, and 2:1) revealed multiple stable entrainment modes for each value of nutlin concentration and period (Figures 3D and 3E). Model simulation of cells with different initial p53 levels confirmed this behavior. For example, depending on their initial condition, cells were entrained to either the 1:2 or 1:1 mode at T_{ext} = 3.6 h (Figure 3F, top) and to either 3:2 or 2:1 at T_{ext} = 9.8 h (Figure 3F, bottom). We next computed the Arnold tongues that represent various entrainment modes as a function of nutlin concentration and external period (Figure 3G). The main Arnold tongues (1:1, 1:2, 3:2, and 2:1) were observed in addition to several higher-order ones (in green). Here, frequency pulling can be visualized as the broadening of Arnold tongues, where an increase of coupling strength (achieved by high concentration of nutlin) enables entrainment at frequencies further from the main p:q ratios (see broadening of the 1:1 tongue at nutlin concentrations of 1 and 2 μM).

Mode hopping and period doubling in p53 dynamics

A subset of cells did not commit to a single entrainment mode, as was evidenced by a non-rational p:q ratio (Figures 3D and 3E). Such ratios can emerge from complex non-linear dynamics, including mode hopping, period doubling, and chaos. Mode hopping occurs when oscillators switch between two stable entrainment modes, usually due to stochastic noise. Period-doubling bifurcations are characterized by patterns of alternating amplitudes, resulting in the major repeating unit of the trajectory having double the period of the peak-to-peak interval of successive pulses.

Simulating the ODE model with Langevin noise revealed mode hopping between states (Figure 4A, top). As expected, increasing the noise level led to more frequent jumps between modes (Figure 4A, bottom). At 2.5 and 11 h, the model also predicted the presence of period-doubling traces (Figure 4B). We used the algorithm described in Figure 3 to identify such potential behaviors in the experimental data for cells with non-rational p:q ratios taken from Figures 3D and 3E. If the period switched between two stable states, the algorithm classified it as mode hopping. If the height of successive peaks differed by more than 30%, the algorithm classified the dynamics as period doubling. In agreement with the model simulations, single-cell traces displayed mode-hopping (Figure 4C) and period-doubling (Figure 4D) dynamics. Overall, we detected mode hopping at all nutlin periods except 4 h, and period doublings were seen in a very small percentage of cells across all conditions (Figures 4E and 4F). A subset of traces did not fall into any of these categories (Figures 4E and 4F, unclassified). Within the fraction of unclassified cells, we observed a broad and relatively flat distribution of peak-to-peak distances (Figure 4G) compared with the distribution of peaks for the entrained fraction (Figure 4H). Such a wide spectrum of frequencies may result from traces undergoing an unpredictable and non-repeating behavior, known as chaos, which we further investigated below.

Proposition of chaos in p53 dynamics

Inspection of unclassified traces revealed pairs of traces that initially showed similar behaviors but diverged with time, resulting in completely unrelated dynamics (Figures 5A and 5B). Such behaviors are consistent with and suggest chaotic dynamics. Simulation of the model at T_{ext} = 11 h with Langevin noise also revealed traces with almost identical initial dynamics that diverge with time (Figure 5C). The Lyapunov exponent that quantifies the separation of the traces was positive both for simulated (Figure 5D) and experimental traces (Figure S3) (0.03 and 0.08 h^{-1}, respectively; see STAR Methods), as expected mathematically from chaos. Furthermore, plotting the traces in the phase space spanned by p53 and Mdm2 revealed a strange attractor, a characteristic of chaotic behavior (Figure 5E).

A cascade of period-doubling bifurcations is one of the possible routes to chaos.[53,54] We therefore asked whether such a stereotypical transition can be identified in our model and experimental data. We computed the bifurcation diagram to visualize how the amplitude of p53 peaks varies as nutlin concentration increases (Figure 5F). The model predicted a cascade of period doublings followed by a chaotic regime (Figure 5F, dense regions), which eventually transitions into 1:1: entrainment, dictated by the period of nutlin. A similar transition—from regular periodic oscillations (at 0.25 μM nultin), to period doubling and chaos (co-occurring at 0.5 μM nutlin), and to 1:1 entrainment (at 2 μM nutlin)—was also identified experimentally (Figure 5G). Supported by the model, we hypothesize that these traces of p53 might be the first chaotic signatures observed in the p53 system.

DISCUSSION

The emergence of oscillations in transcription factors has been well established for two decades, but to what degree this behavior can be externally controlled is still not fully resolved. In this work, we combined principles from the theory of entrainment and live imaging to study the ability of oscillatory p53 to entrain to an external oscillator. Single-cell traces of p53

(E) Same as (D) at a fixed T_{ext} = 11 h across different nutlin concentrations.
(F) Model simulation predicting multi-stability for two pairs of simulated cells; yellow/purple and red/blue. Dashed lines indicate time of nutlin pulses.
(G) Computed Arnold tongues across the nutlin concentrations and T_{ext}, explored experimentally. p:q ratios (1:1, 1:2, 3:2, and 2:1) were assigned with a tolerance of ±1%. Black dots indicate the experimental conditions used in this study. Multi-stability is observed in regions of overlapping tongues (squares 1 and 2, corresponding to the traces in F).

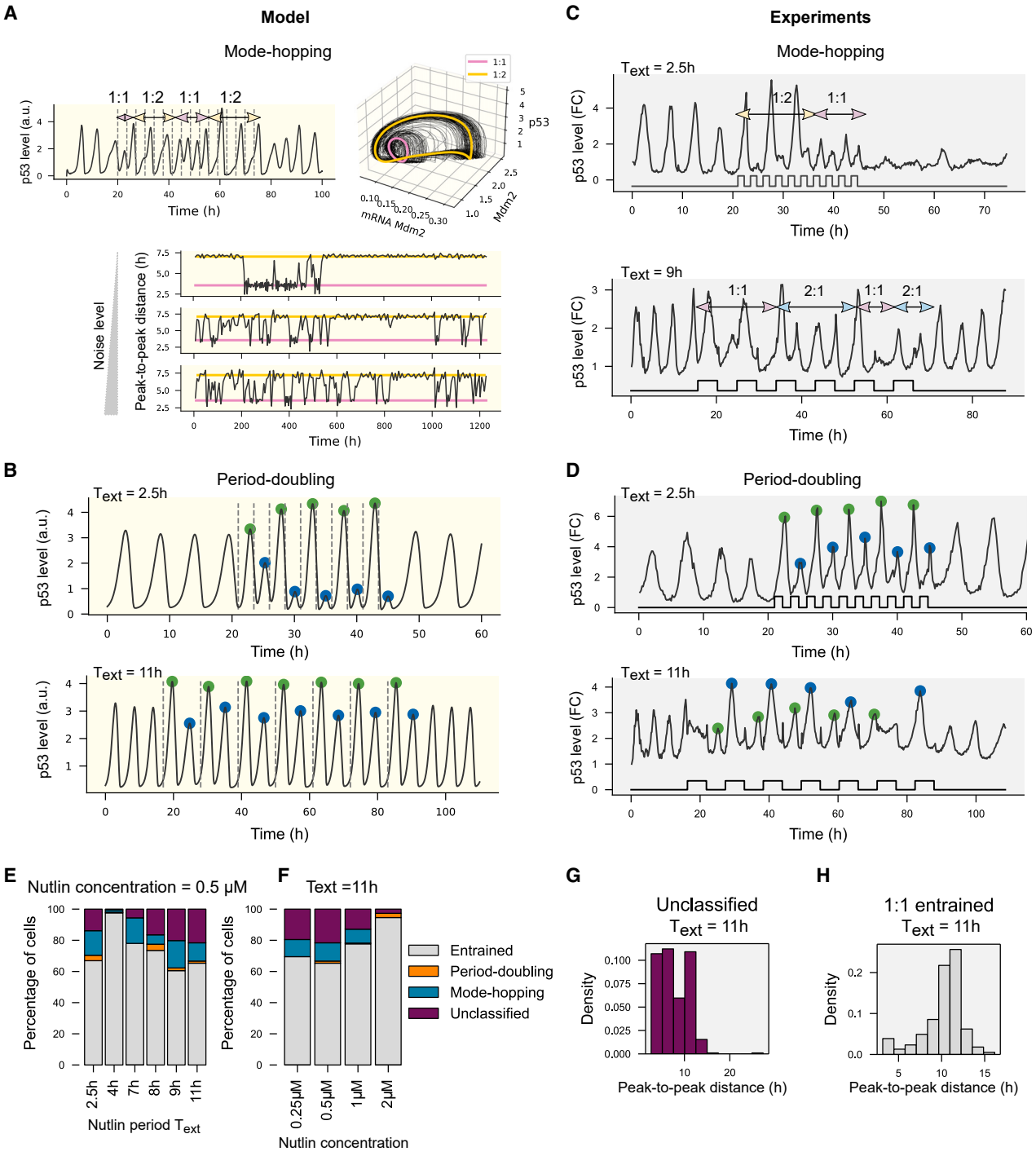

Figure 4. p53 can exhibit complex non-linear dynamics, including mode hopping and period doubling

(A) Model simulations exhibit mode hopping between entrainment modes. Simulations were carried out at T_{ext} = 3.5 h, with addition of Langevin noise. Top-left: single cell trace shows transitions between 1:2 and 1:1 mode. Top-right: three dimensional (3D) trajectories of p53, Mdm2 and mRNA Mdm2 (black) switching between the two deterministic stable trajectories; 1:1 (pink) and 1:2 (yellow). Bottom: peak-to-peak distance of p53 as a function of time (black). Increasing the noise level increases the frequency of transitions between the two stable modes (yellow and pink lines).

(B) Model simulations exhibit period doubling at T_{ext} = 2.5 h and T_{ext} = 11 h.

(C) Examples of p53 traces exhibiting mode hopping at T_{ext} = 2.5 h and T_{ext} = 9 h. Experimental p53 levels are presented in FC. Experimental versus model traces are distinguished with gray and yellow backgrounds, respectively.

(D) Examples of p53 traces exhibiting period doubling at T_{ext} = 2.5 h and T_{ext} = 11 h. Blue and green dots represent peaks of oscillations with two distinct amplitudes.

(legend continued on next page)

oscillations responding to an external oscillator of varying periods and strengths allowed a comprehensive investigation of the wide range of possible dynamical behaviors in this system. Using a predictive ODE model of the feedbacks controlling p53 levels and experimental validations, we identified multiple modes of entrainment as well as transitions to complex nonlinear behaviors, including period doubling, mode hopping, and chaos (Figures 4 and 5). Entertainment was found in other biological systems. However, most biological oscillators can entrain to a relatively narrow range of external periods. For example, circadian clocks in rodents can be entrained to light-dark cycles, with deviations of 2 h from the endogenous period of 24 h. An increase in input strength only minimally stretches this range.[55] Predictions of entrainment of the mammalian cell cycle via the circadian clock proteins Wee1, Cyclin E, or p21 also estimate narrow ranges of entrainment at 24 and 48 h.[9,56,57] Although heterogeneity and deviations from entrainment were also observed for periods far from p53's natural oscillations (Figures 2 and 3D), a stronger input was able to overcome that (Figure 3E). In this study, we used a drug as the external oscillator; however, periodical changes can also be obtained naturally by the environment through changes in oxygen levels, hormones, or nutrient availability. The ability of the p53 oscillator to entrain to a large range of frequencies might be an efficient mechanism for integrating and responding to multiple signals simultaneously.[58,59]

In our experimental system, isogenic populations of cells exhibited a mix of entrainment modes as well as complex nonlinear behaviors. Such heterogeneity can result from stochastic fluctuations in protein levels of individual cells or arise due to cell-intrinsic factors such as cell-cycle phase, cell size, or other morphological features. Traces exhibiting jumps between entrainment modes (mode hopping), and the model predicting that a single cell will display increasing rates of jumps between modes for increasing noise level, supports the co-existence of multiple stable states. From an experimental perspective, identifying the origin of heterogeneity in the regimes of entrainment is a complicated task. It would require measuring various cell-intrinsic factors descriptive of cell state and correlating them with the consequent dynamical behavior. Still, even with such measurements, it is rarely the case that a single factor is responsible for a specific behavior. Hormoz et al.[60] published a method to infer cell state transition dynamics from lineage trees and endpoint single cell measurements. Similar experimental approaches combining lineage tracing of individual cells over multiple generations, together with measurements of various cellular and molecular feature and protein dynamics, will be required to better understand the reasons for heterogeneity in the entrainment modes of p53 between individual cells.

Frequency modulation of transcription factors is often used to control gene expression,[61,62] and entrainment may further allow transcription factors to adjust their gene expression patterns to external oscillating inputs. Resetting and entrainment of the NF-κB oscillator was shown to be a useful mechanism for cells to synchronize their gene expression downstream of NF-κB.[17] Mode hopping in the NF-κB system also allows different regulation across different frequency-sensitive promoters, in which a high-affinity promoter is induced under both frequencies but a low-affinity promoter is induced only under low frequencies.[63] Measurements of p53 target genes will be required to determine whether similar behaviors also exist in this system. In addition, compared with other oscillatory systems, the Arnold tongues capturing p53 entertainment indicate a rich and diverse array of dynamical responses.[63] Multiple Arnold tongues might exist in other less-studied oscillating biological systems and the biological advantage of such diverse dynamical behavior for p53, or potentially for other oscillatory factors, remains an open question.

Characterizing the type of complex dynamics in traces with significant amounts of stochasticity is challenging.[64] Although we cannot conclusively state that we observe chaotic dynamics in the experimental p53 traces, simulation of our model resulted in a positive Lyapunov exponent and a strange attractor in the phase space of p53 and Mdm2, which are strong predictors that the p53 network can indeed develop chaotic dynamics. Moreover, the identification of overlapping Arnold tongues, the observation of mode hopping and period doublings, and as our findings of similar traces that diverge in time, all provide unprecedented and valuable support for chaos. These findings encourage further investigations and suggest specific parameter ranges for exploration, effectively pinpointing the potential region where chaotic behavior could be detected. Additionally, they suggest that the design of the p53 network may lead to a relatively narrow chaotic window, as complex dynamics are swiftly replaced by robust entrainment, which could potentially serve to stabilize p53 oscillations, especially in the face of external stressors. Combinatorial therapies are now widely used in the clinic. In the case of p53, one can imagine combining IR with other stressors, or with drugs that inhibit Mdm2, like the one used in this study to control p53 dynamics and enhance its function.[65] Our ability to now understand and predict how the p53 oscillator responds to various drug doses and frequencies is critical for designing new protocols that trigger dynamical behaviors associated with the destruction of cancer cells. Taken together, this work conclusively reveals the potential for coupling oscillatory signals in biology and suggests a way to effectively control p53 concentration dynamics at the single-cell level.

RESOURCE AVAILABILITY

Lead contact

Further information and requests for resources and reagents should be directed to and will be fulfilled by the lead contact, Galit Lahav (galit@hms.harvard.edu).

Materials availability

All materials are either commercially available or can be available upon request.

(E) Percentage of complex dynamics at a fixed nutlin concentration (0.5 μM) across T_{ext} values. Gray bars refer to the entrained states (yellow, purple, pink, and blue bars in Figures 3D, 3E, and 3G). Colored bars represent the non-entrained traces (corresponding to the gray bars in Figures 3D and 3E).
(F) Same as (E) at a fixed T_{ext} (11 h) across different nutlin concentrations.
(G) Distribution of the peak-to-peak distance in the unclassified population of cells with T_{ext} = 11 h and nutlin concentration = 0.5 μM.
(H) Distribution of the peak-to-peak distance of the 1:1 entrained population of cells at T_{ext} = 11 h and nutlin concentration = 0.5 μM.

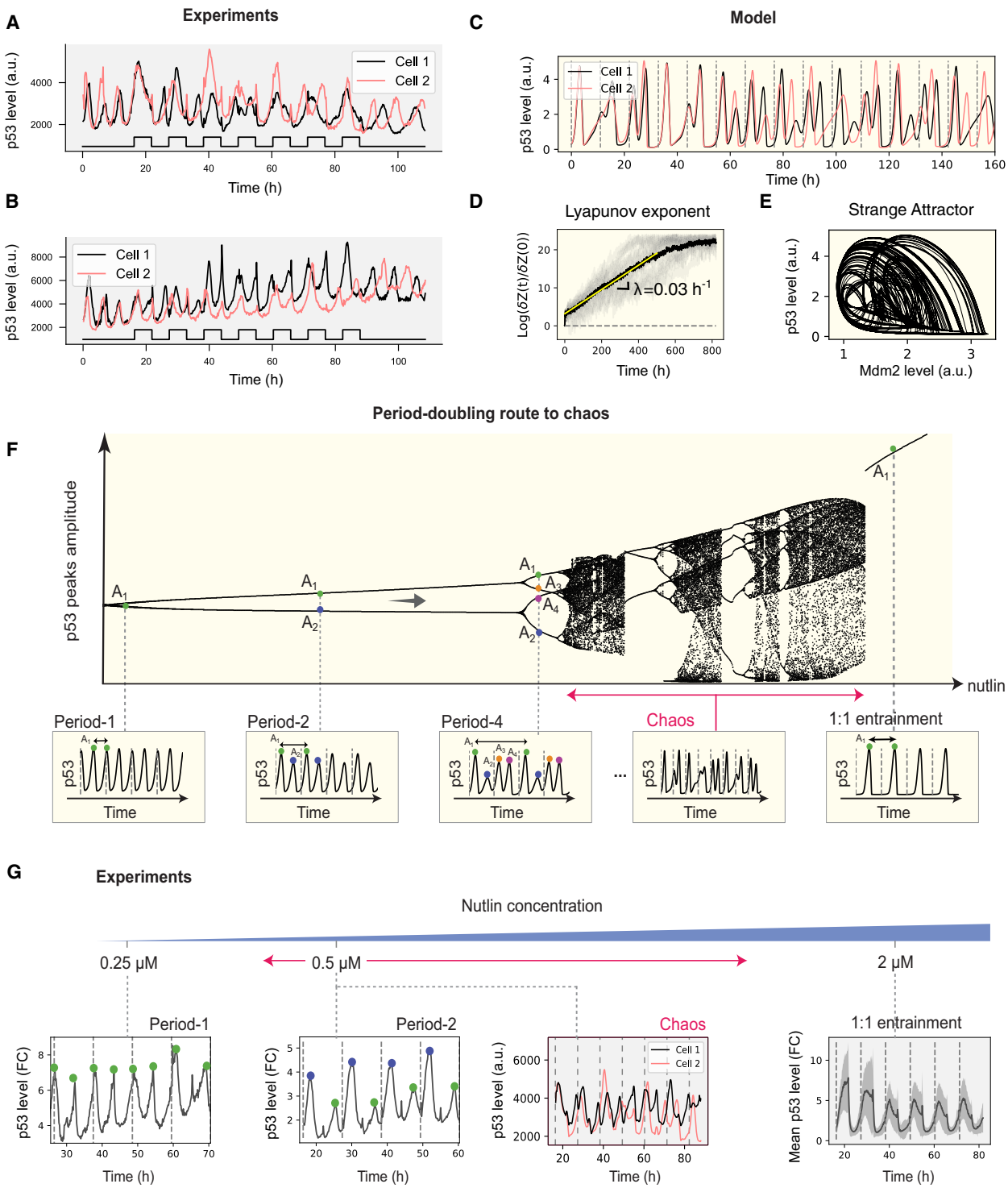

Figure 5. p53 shows signs of chaotic behavior

(A and B) Two examples of unclassified pairs of cells exhibiting similar initial dynamics that diverge with time, an behavior indicative of chaos (see also Figure S3). Experimental versus model traces are distinguished with gray and yellow backgrounds, respectively.

(C) Simulation of two traces at T_{ext} = 11 h and f = 48% with similar initial conditions, exhibiting divergence of the trajectories over time.

(D) 20 simulations with nearly identical initial conditions (separated by 10^{-10}), tracking their divergence over time (gray traces). The averaged divergence is depicted as a black line. A linear fit (yellow line) is applied to the system before it reaches saturation. The slope of this line ($\lambda = 0.03\ h^{-1}$) represents the Lyapunov exponent, which, being positive, confirms the chaotic nature of the traces.

(E) The trajectory plotted in the two-dimensional (2D) plane of Mdm2, p53 exhibits a strange attractor.

(legend continued on next page)

Data and code availability

- All data reported in this paper will be shared by the lead contact upon request.
- All original code has been deposited at Zenodo and is publicly available as of the date of publication. DOIs are listed in the key resources table.
- Any additional information required to reanalyze the data reported in this paper is available from the lead contact upon request.

ACKNOWLEDGMENTS

We thank members of the Lahav lab for discussion and critical comments on the manuscript. This project was supported by funding from the National Institutes of Health grant R35 GM139572 (G.L.), the Ludwig Center at Harvard (G.L.), the European Research Council (ERC) no. 740704 (M.H.J.), the Lundbeck Foundation (grant: R347-2020-2250) (M.H.J.), the Independent Research Fund Denmark (grant: 9040-00116B) (M.H.J.), and the Novo Nordisk Foundation (grant: NNF20OC0064978) (M.H.J.).

AUTHOR CONTRIBUTIONS

A. Jiménez, A. Jambhekar, M.S.H., M.H.J., and G.L. – planning and conceptualization; A. Jiménez, A.L., M.S.H., and L.M. – simulations and mathematical analysis; A. Jiménez, A. Jambhekar, C.S., and G.L. – experimental design; A. Jiménez – carrying out the experiments; A. Jiménez, A.L., M.S.H., A. Jambhekar, M.H.J., and G.L. – analysis of the experimental results; A. Jiménez, A.L., M.S.H., A. Jambhekar, M.H.J., and G.L. – writing the manuscript; A. Jiménez, A.L., M.S.H., A. Jambhekar, M.H.J., and G.L. – editing the manuscript.

DECLARATION OF INTERESTS

The authors declare no competing interests.

STAR★METHODS

Detailed methods are provided in the online version of this paper and include the following:

- KEY RESOURCES TABLE
- EXPERIMENTAL MODEL
  - Cell-lines
- METHOD DETAILS
  - Ionizing irradiation
  - Live-cell microscopy
  - Microfluidics device
  - Mathematical model of a single nutlin pulse
  - Deriving 1:1 Entrainment from PRCs
  - Mathematical model of periodic nutlin pulses
- QUANTIFICATION AND STATISTICAL ANALYSIS
  - Single cell tracking and analysis
  - Classification of entrainment states
  - Computation of the Lyapunov exponent

SUPPLEMENTAL INFORMATION

Supplemental information can be found online at https://doi.org/10.1016/j.cels.2024.09.001.

Received: January 9, 2024
Revised: June 25, 2024
Accepted: September 12, 2024
Published: October 4, 2024

REFERENCES

1. Nelson, D.E., Ihekwaba, A.E.C., Elliott, M., Johnson, J.R., Gibney, C.A., Foreman, B.E., Nelson, G., See, V., Horton, C.A., Spiller, D.G., et al. (2004). Oscillations in NF-κB Signaling Control the Dynamics of Gene Expression. Science *306*, 704–708. https://doi.org/10.1126/science.1099962.
2. Gonze, D., Halloy, J., and Goldbeter, A. (2002). Robustness of circadian rhythms with respect to molecular noise. Proc. Natl. Acad. Sci. USA *99*, 673–678.
3. Hoffmann, A., Levchenko, A., Scott, M.L., and Baltimore, D. (2002). The IκB-NF-κB Signaling Module: Temporal Control and Selective Gene Activation. Science *298*, 1241–1245. https://doi.org/10.1126/science.1071914.
4. Lahav, G., Rosenfeld, N., Sigal, A., Geva-Zatorsky, N., Levine, A.J., Elowitz, M.B., and Alon, U. (2004). Dynamics of the p53-Mdm2 feedback loop in individual cells. Nat. Genet. *36*, 147–150. https://doi.org/10.1038/ng1293.
5. Chen, Y., Kim, J.K., Hirning, A.J., Josić, K., and Bennett, M.R. (2015). Emergent genetic oscillations in a synthetic microbial consortium. Science *349*, 986–989. https://doi.org/10.1126/science.aaa3794.
6. Yang, Q., and Ferrell, J.E.J. (2013). The Cdk1-APC/C cell cycle oscillator circuit functions as a time-delayed, ultrasensitive switch. Nat. Cell Biol. *15*, 519–525. https://doi.org/10.1038/ncb2737.
7. Heltberg, M.S., Lucchetti, A., Hsieh, F.-S., Minh Nguyen, D.P.M., Chen, S.-H., and Jensen, M.H. (2022). Enhanced DNA repair through droplet formation and p53 oscillations. Cell *185*, 4394–4408.e10. https://doi.org/10.1016/j.cell.2022.10.004.
8. Jiménez, A., Lu, Y., Jambhekar, A., and Lahav, G. (2022). Principles, mechanisms and functions of entrainment in biological oscillators. Interface Focus *12*, 20210088. https://doi.org/10.1098/rsfs.2021.0088.
9. Yan, J., and Goldbeter, A. (2019). Robust synchronization of the cell cycle and the circadian clock through bidirectional coupling. J. R. Soc. Interface *16*, 20190376. https://doi.org/10.1098/rsif.2019.0376.
10. Heltberg, M.L., Krishna, S., Kadanoff, L.P., and Jensen, M.H. (2021). A tale of two rhythms: Locked clocks and chaos in biology. Cell Syst. *12*, 291–303. https://doi.org/10.1016/j.cels.2021.03.003.
11. Gutu, N., Nordentoft, M.S., Kuhn, M., Ector, C., Finger, A.-M., Heltberg, M.S., Jensen, M.H., Keilholz, U., Herzel, H., and Granada, A.E. (2024). Circadian Coupling Orchestrates Cell Growth. Preprint at bioRxiv. https://doi.org/10.1101/2024.05.18.594797.
12. Jalife, J. (1984). Mutual entrainment and electrical coupling as mechanisms for synchronous firing of rabbit sino-atrial pace-maker cells. J. Physiol. *356*, 221–243. https://doi.org/10.1113/jphysiol.1984.sp015461.
13. Plautz, J.D., Kaneko, M., Hall, J.C., and Kay, S.A. (1997). Independent Photoreceptive Circadian Clocks Throughout Drosophila. Science *278*, 1632–1635. https://doi.org/10.1126/science.278.5343.1632.
14. Zeng, H., Qian, Z., Myers, M.P., and Rosbash, M. (1996). A light-entrainment mechanism for the Drosophila circadian clock. Nature *380*, 129–135. https://doi.org/10.1038/380129a0.
15. Thommen, Q., Pfeuty, B., Schatt, P., Bijoux, A., Bouget, F.-Y., and Lefranc, M. (2015). Probing entrainment of Ostreococcus tauri circadian clock by green and blue light through a mathematical modeling approach. Front. Genet. *6*, 65. https://doi.org/10.3389/fgene.2015.00065.
16. Granada, A.E., and Herzel, H. (2009). How to Achieve Fast Entrainment? The Timescale to Synchronization. PLoS ONE *4*, e7057. https://doi.org/10.1371/journal.pone.0007057.

(F) Period-doubling route to chaos emerges from the model as a cascade of period-doubling bifurcations (period-1, period-2, period-4, …, to chaos). For high nutlin concentrations, the 1:1 entrainment mode prevails.
(G) Examples of experimental p53 traces matching the theoretical transition to chaos at increasing nutlin concentration and fixed T_{ext} = 11 h.

17. Kellogg, R.A., and Tay, S. (2015). Noise Facilitates Transcriptional Control under Dynamic Inputs. Cell *160*, 381–392. https://doi.org/10.1016/j.cell.2015.01.013.

18. Cross, F.R., and Siggia, E.D. (2005). Mode locking the cell cycle. Phys. Rev. E Stat. Nonlin. Soft Matter Phys. *72*, 021910. https://doi.org/10.1103/physreve.72.021910.

19. Pikovsky, A., Rosenblum, M., and Kurths, J. (2001). Synchronization: A Universal Concept in Nonlinear Sciences (Cambridge University Press). https://doi.org/10.1017/cbo9780511755743.

20. Mork, J., Semkow, M., and Tromborg, B. (1990). Measurement and theory of mode hopping in external cavity lasers. In CFQ4 (Optica Publishing Group).

21. Martin, K.I., Clarkson, W.A., and Hanna, D.C. (1997). Self-suppression of axial mode hopping by intracavity second-harmonic generation. Opt. Lett. *22*, 375–377. https://doi.org/10.1364/ol.22.000375.

22. Heltberg, M., Kellogg, R.A., Krishna, S., Tay, S., and Jensen, M.H. (2016). Noise Induces Hopping between NF-κB Entrainment Modes. Cell Syst. *3*, 532–539.e3. https://doi.org/10.1016/j.cels.2016.11.014.

23. Strogatz, S.H. (1996). Nonlinear Dynamics and Chaos (CRC Press).

24. Glass, L., and Mackey, M.C. (1988). From Clocks to Chaos: the Rhythms of Life (Princeton University Press).

25. Jensen, M.H., Bak, P., and Bohr, T. (1984). Transition to chaos by interaction of resonances in dissipative systems. I. Circle maps. Phys. Rev. A *30*, 1960–1969. https://doi.org/10.1103/physreva.30.1960.

26. Stavans, J., Heslot, F., and Libchaber, A. (1985). Fixed Winding Number and the Quasiperiodic Route to Chaos in a Convective Fluid. Phys. Rev. Lett. *55*, 596–599. https://doi.org/10.1103/physrevlett.55.596.

27. Gwinn, E.G., and Westervelt, R.M. (1986). Frequency Locking, Quasiperiodicity, and Chaos in Extrinsic Ge. Phys. Rev. Lett. *57*, 1060–1063. https://doi.org/10.1103/physrevlett.57.1060.

28. Brown, S.E., Mozurkewich, G., and Grüner, G. (1984). Subharmonic Shapiro Steps and Devil's-Staircase Behavior in Driven Charge-Density-Wave Systems. Phys. Rev. Lett. *52*, 2277–2280. https://doi.org/10.1103/physrevlett.52.2277.

29. Zeng, W.Z., Glass, L., and Shrier, A. (1991). Evolution of rhythms during periodic stimulation of embryonic chick heart cell aggregates. Circ. Res. *69*, 1022–1033. https://doi.org/10.1161/01.res.69.4.1022.

30. Mondragón-Palomino, O., Danino, T., Selimkhanov, J., Tsimring, L., and Hasty, J. (2011). Entrainment of a Population of Synthetic Genetic Oscillators. Science *333*, 1315–1319. https://doi.org/10.1126/science.1205369.

31. Krishna, S., Jensen, M.H., and Sneppen, K. (2006). Minimal model of spiky oscillations in NF-κB signaling. Proc. Natl. Acad. Sci. USA *103*, 10840–10845. https://doi.org/10.1073/pnas.0604085103.

32. Sanchez, P.G.L., Mochulska, V., Mauffette Denis, C.M., Mönke, G., Tomita, T., Tsuchida-Straeten, N., Petersen, Y., Sonnen, K., François, P., and Aulehla, A. (2022). Arnold tongue entrainment reveals dynamical principles of the embryonic segmentation clock. eLife *11*, e79575. https://doi.org/10.7554/elife.79575.

33. Oren, M., and Prives, C. (2024). p53: A tale of complexity and context. Cell *187*, 1569–1573. https://doi.org/10.1016/j.cell.2024.02.043.

34. Batchelor, E., Loewer, A., Mock, C., and Lahav, G. (2011). Stimulus-dependent dynamics of p53 in single cells. Mol. Syst. Biol. *7*, 488. https://doi.org/10.1038/msb.2011.20.

35. Stewart-Ornstein, J., Iwamoto, Y., Miller, M.A., Prytyskach, M.A., Ferretti, S., Holzer, P., Kallen, J., Furet, P., Jambhekar, A., Forrester, W.C., et al. (2021). p53 dynamics vary between tissues and are linked with radiation sensitivity. Nat. Commun. *12*, 898. https://doi.org/10.1038/s41467-021-21145-z.

36. Stewart-Ornstein, J., Cheng, H.W.J., and Lahav, G. (2017). Conservation and Divergence of p53 Oscillation Dynamics across Species. Cell Syst. *5*, 410–417.e4. https://doi.org/10.1016/j.cels.2017.09.012.

37. Batchelor, E., Mock, C.S., Bhan, I., Loewer, A., and Lahav, G. (2008). Recurrent Initiation: A Mechanism for Triggering p53 Pulses in Response to DNA Damage. Mol. Cell *30*, 277–289. https://doi.org/10.1016/j.molcel.2008.03.016.

38. Hamstra, D.A., Bhojani, M.S., Griffin, L.B., Laxman, B., Ross, B.D., and Rehemtulla, A. (2006). Real-time evaluation of p53 oscillatory behavior in vivo using bioluminescent imaging. Cancer Res. *66*, 7482–7489. https://doi.org/10.1158/0008-5472.can-06-1405.

39. Wu, X., Bayle, J.H., Olson, D., and Levine, A.J. (1993). The p53-mdm-2 autoregulatory feedback loop. Genes Dev. *7*, 1126–1132. https://doi.org/10.1101/gad.7.7a.1126.

40. Fuchs, S.Y., Adler, V., Buschmann, T., Wu, X., and Ronai, Z. (1998). Mdm2 association with p53 targets its ubiquitination. Oncogene *17*, 2543–2547. https://doi.org/10.1038/sj.onc.1202200.

41. Honda, R., Tanaka, H., and Yasuda, H. (1997). Oncoprotein MDM2 is a ubiquitin ligase E3 for tumor suppressor p53. FEBS Lett. *420*, 25–27. https://doi.org/10.1016/s0014-5793(97)01480-4.

42. Haupt, Y., Maya, R., Kazaz, A., and Oren, M. (1997). Mdm2 promotes the rapid degradation of p53. Nature *387*, 296–299. https://doi.org/10.1038/387296a0.

43. Kubbutat, M.H., Jones, S.N., and Vousden, K.H. (1997). Regulation of p53 stability by Mdm2. Nature *387*, 299–303. https://doi.org/10.1038/387299a0.

44. Purvis, J.E., Karhohs, K.W., Mock, C., Batchelor, E., Loewer, A., and Lahav, G. (2012). p53 dynamics control cell fate. Science *336*, 1440–1444. https://doi.org/10.1126/science.1218351.

45. Harton, M.D., Koh, W.S., Bunker, A.D., Singh, A., and Batchelor, E. (2019). p53 pulse modulation differentially regulates target gene promoters to regulate cell fate decisions. Mol. Syst. Biol. *15*, e8685. https://doi.org/10.15252/msb.20188685.

46. Hafner, A., Stewart-Ornstein, J., Purvis, J.E., Forrester, W.C., Bulyk, M.L., and Lahav, G. (2017). p53 pulses lead to distinct patterns of gene expression albeit similar DNA-binding dynamics. Nat. Struct. Mol. Biol. *24*, 840–847. https://doi.org/10.1038/nsmb.3452.

47. Vassilev, L.T., Vu, B.T., Graves, B., Carvajal, D., Podlaski, F., Filipovic, Z., Kong, N., Kammlott, U., Lukacs, C., Klein, C., et al. (2004). *In vivo* activation of the p53 pathway by small-molecule antagonists of MDM2. Science *303*, 844–848. https://doi.org/10.1126/science.1092472.

48. Stewart-Ornstein, J., and Lahav, G. (2017). p53 dynamics in response to DNA damage vary across cell lines and are shaped by efficiency of DNA repair and activity of the kinase ATM. Sci. Signal. *10*, eaah6671. https://doi.org/10.1126/scisignal.aah6671.

49. Reyes, J., Chen, J.-Y., Stewart-Ornstein, J., Karhohs, K.W., Mock, C.S., and Lahav, G. (2018). Fluctuations in p53 Signaling Allow Escape from Cell-Cycle Arrest. Mol. Cell *71*, 581–591.e5. https://doi.org/10.1016/j.molcel.2018.06.031.

50. Mengel, B., Hunziker, A., Pedersen, L., Trusina, A., Jensen, M.H., and Krishna, S. (2010). Modeling oscillatory control in NF-κB, p53 and Wnt signaling. Curr. Opin. Genet. Dev. *20*, 656–664. https://doi.org/10.1016/j.gde.2010.08.008.

51. Pfeuty, B., Thommen, Q., and Lefranc, M. (2011). Robust entrainment of circadian oscillators requires specific phase response curves. Biophys. J. *100*, 2557–2565. https://doi.org/10.1016/j.bpj.2011.04.043.

52. Izhikevich, E.M. (2006). Dynamical Systems in Neuroscience: The Geometry of Excitability and Bursting (The MIT Press).

53. Glazier, J.A., Jensen, M.H., Libchaber, A., and Stavans, J. (1986). Structure of Arnold tongues and the f(α) spectrum for period doubling: Experimental results. Phys. Rev. A Gen. Phys. *34*, 1621–1624. https://doi.org/10.1103/physreva.34.1621.

54. Giglio, M., Musazzi, S., and Perini, U. (1981). Transition to Chaotic Behavior via a Reproducible Sequence of Period-Doubling Bifurcations. Phys. Rev. Lett. *47*, 243–246. https://doi.org/10.1103/physrevlett.47.243.

55. Eckel-Mahan, K., and Sassone-Corsi, P. (2015). Phenotyping Circadian Rhythms in Mice. Curr. Protoc. Mouse Biol. *5*, 271–281. https://doi.org/10.1002/9780470942390.mo140229.

56. Leung, C., Gérard, C., and Gonze, D. (2023). Modeling the Circadian Control of the Cell Cycle and Its Consequences for Cancer Chronotherapy. Biology *12*, 612. https://doi.org/10.3390/biology12040612.

57. Gérard, C., and Goldbeter, A. (2012). Entrainment of the Mammalian Cell Cycle by the Circadian Clock: Modeling Two Coupled Cellular Rhythms. PLoS Comput. Biol. *8*, e1002516. https://doi.org/10.1371/journal.pcbi.1002516.

58. Heltberg, M.S., Jiang, Y., Fan, Y., Zhang, Z., Nordentoft, M.S., Lin, W., Qian, L., Ouyang, Q., Jensen, M.H., and Wei, P. (2023). Coupled oscillator cooperativity as a control mechanism in chronobiology. Cell Syst. *14*, 382–391.e5. https://doi.org/10.1016/j.cels.2023.04.001.

59. Jeong, E.M., Song, Y.M., and Kim, J.K. (2022). Combined multiple transcriptional repression mechanisms generate ultrasensitivity and oscillations. Interface Focus *12*, 20210084. https://doi.org/10.1098/rsfs.2021.0084.

60. Hormoz, S., Singer, Z.S., Linton, J.M., Antebi, Y.E., Shraiman, B.I., and Elowitz, M.B. (2016). Inferring Cell-State Transition Dynamics from Lineage Trees and Endpoint Single-Cell Measurements. Cell Syst. *3*, 419–433.e8. https://doi.org/10.1016/j.cels.2016.10.015.

61. Cai, L., Dalal, C.K., and Elowitz, M.B. (2008). Frequency-modulated nuclear localization bursts coordinate gene regulation. Nature *455*, 485–490. https://doi.org/10.1038/nature07292.

62. Ashall, L., Horton, C.A., Nelson, D.E., Paszek, P., Harper, C.V., Sillitoe, K., Ryan, S., Spiller, D.G., Unitt, J.F., Broomhead, D.S., et al. (2009). Pulsatile stimulation determines timing and specificity of NF-kappaB-dependent transcription. Science *324*, 242–246. https://doi.org/10.1126/science.1164860.

63. Heltberg, M.L., Krishna, S., and Jensen, M.H. (2019). On chaotic dynamics in transcription factors and the associated effects in differential gene regulation. Nat. Commun. *10*, 71. https://doi.org/10.1038/s41467-018-07932-1.

64. Amon, A., and Lefranc, M. (2004). Topological signature of deterministic chaos in short nonstationary signals from an optical parametric oscillator. Phys. Rev. Lett. *92*, 094101. https://doi.org/10.1103/physrevlett.92.094101.

65. Levine, A.J. (2022). Targeting the P53 Protein for Cancer Therapies: The Translational Impact of P53 Research. Cancer Res. *82*, 362–364. https://doi.org/10.1158/0008-5472.can-21-2709.

STAR★METHODS

KEY RESOURCES TABLE

REAGENT or RESOURCE	SOURCE	IDENTIFIER
Deposited data		
Code for single cell analysis	This paper	Zenodo: https://doi.org/10.5281/zenodo.13338246
Experimental models: Cell lines		
MCF7p53YFP	Stewart-Ornstein and Lahav[48]	N/A
Chemicals, Peptides and Recombinant proteins		
Nutlin3A	Sigma	SML0580
Software and algorithms		
Custom Matlab Scriptsimage analysis	Stewart-Ornstein and Lahav[48]	N/A
Custom Python Scriptsentrainment analysis	This paper	https://doi.org/10.5281/zenodo.13338246

EXPERIMENTAL MODEL

Cell-lines

MCF7 cells were grown in RPMI supplemented with 10% FBS, 100U/mL penicillin, 100mg/mL streptomycin and 250ng/mL fungizone (Gemini Bio-Products).

Exogenous expression of p53 in MCF7 was achieved by infecting cells with lentivirus containing p53-YFP under the ubiquitin promoter as was previously described.[48] The p53-YFP constructs contained neomycin resistance gene. Cells were subsequently cloned, and single cell clones were expanded and screened for marker expression.

METHOD DETAILS

Ionizing irradiation

Cells were irradiated with 10Gy using a RS-2000 XRay irradiator.

Live-cell microscopy

For microscopy, RPMI without phenol-red was supplemented with 5% FBS and 100mg/mL streptomycin and 250ng/mL fungizone. 20K cells were seeded in 35 mm poly-D-lysine-coated glass bottom plates (MatTek Corporation) 2 days prior to imaging. Cells were imaged using a Nikon Eclipse TE-2000 inverted microscope with a 20X Plan Apo objective and a Hammamatsu Orca ER camera, equipped with environmental chamber controlling temperature, atmosphere (5% CO2) and humidity. Images were acquired every 10 min using the MetaMorph Software. Tracking and image-analysis was performed as previously published.[35]

Microfluidics device

The Arduino, an open-source electronics platform, was coupled with a set of hydraulic pumps to control periodic changes from drug-free media to media with Nutlin while cells were under the microscope.

Mathematical model of a single nutlin pulse

Administering a pulse of nutlin at time T_{ON} and washing it at time T_{OFF} is modelled as follows:

$$k_2(t) = \begin{cases} k_2^0, if\ t < T_{ON}\ or\ t > T_{OFF} \\ k_2^1 + (k_2^0 - k_2^1)(1 - e^{-k_8(t-T_{ON})}), if\ T_{ON} < t < T_{OFF} \end{cases}$$

At time T_{ON}, k_2 transitions from its unperturbed value, k_2^0, to k_2^1 (being $k_2^1 < k_2^0$). Following this reset, k_2 undergoes exponential decay with a rate constant of k_8. Subsequently, at time T_{OFF}, k_2 reverts to its original unperturbed value k_2^0.

Deriving 1:1 Entrainment from PRCs

The Poincaré map was defined as the phase of the internal oscillator (with intrinsic period T_{int}) after n pulses of the external oscillator (with period T_{ext}):

$$\theta_{n+1} = \theta_n + PRC(\theta_n) + T_{ext}, mod\ T_{int},$$

where $\theta_n \in [0, T_{int}]$.

When $T_{ext} \approx T_{int}$, the map can be written as:

$$\theta_{n+1} = \theta_n + PRC(\theta_n) + T_{ext} - T_{int}.$$

Therefore, a fixed point θ^* of the map satisfies:

$$\theta^* = \theta^* + PRC(\theta^*) + T_{ext} - T_{int} \Rightarrow PRC(\theta^*) = T_{int} - T_{ext} \quad \text{(criterium 1)}$$

The condition for the fixed point to be stable is:

$$\left|\frac{d\theta_{n+1}}{d\theta_n}\right|_{\theta_n = \theta^*} < 1 \Rightarrow |1 + PR\,C'(\theta^*)| < 1 \Rightarrow -2 < PR\,C'(\theta^*) < 0 \quad \text{(criterium 2)}$$

If the two criteria are satisfied, there exists a phase θ^* such that the internal oscillator is entrained to the external oscillator.

Mathematical model of periodic nutlin pulses

To model periodic pulses of nutlin in the ODE model, the parameter k_2 (t) is assumed to be constant (k_2^0) in zone 1 and zone 3 and sinusoidal in zone 2:

$$k_2(t) = \begin{cases} k_2^0, if\ t < T_{ON}\ or\ t > T_{OFF} \\ k_2^0\left(\frac{f}{2}\left(cos\left(2\pi\frac{(t - T_{ON})}{T_{EXT}}\right) - 1\right) + 1\right), if\ T_{ON} < t < T_{OFF} \end{cases}$$

$k_2(t)$ thus oscillates between the unperturbed state k_2^0 and $(1 - f)\cdot k_2^0$, with f in $[0, 1]$ being the maximal fractional reduction of k_2.

QUANTIFICATION AND STATISTICAL ANALYSIS

Single cell tracking and analysis

Cells were tracked using a semi-automated tracking method, as described in Reyes et al.[49] Code for analyzing single cell data is available at Zenodo (see data and code availability).

Classification of entrainment states

A polynomial function was fitted to the p53 traces from Zone 2 and subtracted from the data to de-trend it. A median filter and a polynomial filter were then applied to smooth the data. Subsequently, the number of p53 peaks were computed making use of the SciPy Python package. Peaks with prominence greater than 20% of the mean prominence were selected. The peak-to-peak distance was extracted from the position of the peaks. The algorithm then checks if the trajectory can be classified as entrained, period-doubling or mode-hopping according to the following criteria:

Period-doubling: If $\frac{|amp_1 - amp_2|}{\sqrt{std(amp_1)^2 + std(amp_2)^2}} > \epsilon_1$ *with* $\epsilon_1 = 2.5$, where (amp_1, amp_2) are the amplitudes of alternating peaks.

Entrained: The entrainment mode (rot, can also be referred to as rotation number) is computed as the ratio of the nutlin period and the weighted mean of the peak-to-peak distances: peaks are given weights proportionally to their index so that the final ones weigh more than the initial ones, which may still be in the transient phase. If $|p/q - rot| < \epsilon_2$ *with* $\epsilon_2 = 0.15$, and if in the second half of Zone 2 there are p p53 peaks per q modes then the trajectory is classified as entrained to mode $\omega = p/q$, where $\omega \in [0.5, 1, 1.5, 2]$.

As stated above, to assign an experimental single cell trace to a specific entrainment mode (i.e p/q ratios 1:1, 1:2, 3:2, 2:1), we applied a tolerance of +/- 15%. To assign entrainment modes to the simulated cells in the computed Arnold Tongues, we applied a tolerance of +/-1% (Figure 3G). Simulated traces can hold a more stringent criteria (1%) since traces can be simulated for longer periods and noise-free, achieving much higher accuracy for defining the correct boundaries of the tongues.

Mode-hopping: For every peak-to-peak distance, $rot_i = \frac{T_{ext}}{peak - to - peak_i}$. If $|\omega - rot_i| < \epsilon_2$, mode ω is detected.

If there are at least 2 modes detected, with the one that occurs most frequently holds for at least M nutlin periods, and the second most frequent holds at least for M-1where M = 1/3 no. nutlin peaks, then the trajectory is classified as mode-hopping.

Unclassified: If a trajectory does not fall into any of the categories described above it is considered unclassified. Within the unclassified traces, the algorithm compares initial 10 timepoints and finds those that have smaller differences. Traces are then visually inspected to find those that have diverging behaviors over time.

Computation of the Lyapunov exponent

To compute the Lyapunov exponent, the system is simulated with a fractional reduction of k_2 of 48%, starting from 2 very close initial conditions x_0 and $x_0 + \epsilon$ (with $\epsilon = 10^{-10}$) for p53, Mdm2-mRNA and Mdm2. The simulation is repeated 20 times, each time with x_0

being the endpoint of the previous simulation. This ensures that the trajectory has reached the stable solution (the strange attractor if it is chaotic dynamics). Then the separation between the two trajectories x_1 and x_2 is computed as $\delta Z\ (t) = |x_1 - x_2|$ where $|\cdot|$ is the vector norm.

The divergence between the two traces therefore corresponds to $div = log(\delta Z(t)\ /\delta Z(0))$.

The mean divergence between the 20 couples of trajectories is computed and finally fit with a linear function, whose slope λ corresponds to the Lyapunov exponent.